THE JOURNAL OF PHYSICAL CHEMISTRY B

Article

pubs.acs.org/JPCB

First-Principles Density Functional Theory (DFT) Study of Gold Nanorod and Its Interaction with Alkanethiol Ligands

Hang Hu,[†] Linda Reven,[‡] and Alejandro Rey*,[†]

[†]Department of Chemical Engineering, McGill University, 845 Sherbrook Street West, Montreal, Quebec, Canada, H3A 0G4

[‡]Department of Chemistry, McGill University, 801 Sherbrooke Street West, Montreal, Quebec Canada, H3A 2K6

ABSTRACT: The structure and mechanical properties of gold nanorods and their interactions with alkenthiolate self-assembled monolayers have been determined using a novel first-principle density functional theory simulation approach. The multifaceted, 1-dimensional, octagonal nanorod has alternate Au100 and Au110 surfaces. The structural optimization of the gold nanorods was performed with a mixed basis: the outermost layer of gold atoms used double-ζ plus polarization (DZP), the layer below used double-ζ (DZ), and the inner layers used single-ζ (SZ). The final structure compares favorably with simulations using DZP for all atoms. Phonon dispersion calculations and *ab initio* molecular dynamics (AIMD) were used to establish the dynamic and thermal stability of the system. From the AIMD simulations it was found that the nanorod system will undergo significant surface reconstruction at 300 K. In addition, when subjected to mechanical stress in the axial direction, the nanorod responds as an orthotropic material, with uniform expansion along the radial direction. The Young's moduli are 207 kbar in the axial direction and 631 kbar in the radial direction. The binding of alkanethiolates, ranging from methanethiol to pentanethiol, caused formation of surface point defects on the Au110 surfaces. On the Au100 surfaces, the defects occurred in the inner layer, creating a small surface island. These defects make positive and negative concavities on the gold nanorod surface, which helps the ligand to achieve a more stable state. The simulation results narrowed significant knowledge gaps on the alkanethiolate adsorption process and on their mutual interactions on gold nanorods. The mechanical characterization offers a new dimension to understand the physical chemistry of these complex nanoparticles.

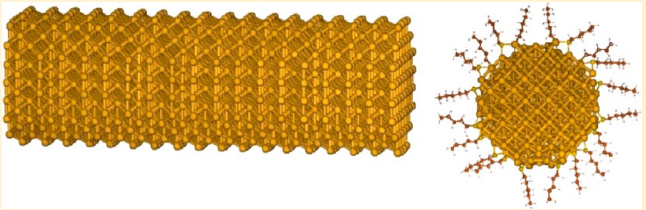

1. INTRODUCTION

Gold nanorods (GNRs) have garnered considerable interest in the research community over the past decades.[1,2] With their highly anisotropic shape and favorable plasmonic properties, GNRs can be used as highly versatile multiplex biosensor assays.[1,2] GNR properties are very sensitive to surface conditions, and even a small shape change can have a large impact on a number of physical and chemical properties.[3] Due to the high surface to volume ratio, GNRs exhibit many unique properties that separate them from bulk materials.[4,5] Simply by varying their size, these nanorods can have a very high selective catalytic efficiency.[2] The emission from a cross section of a gold nanoparticle is a million times stronger than that of typical fluorescent molecules, making it a powerful biomedical imaging tool.[6] Ligand-decorated GNRs can have even greater functionality by generating polymorphic states.[7,8] GNRs are being employed as building blocks in molecular electronics, immobilization of biomolecules, and many other applications.[1,9] Despite their high potential and intense research focus, there is still a knowledge gap with respect to molecular level characterization.

GNRs have a very complex surface structure with corners and edges affecting the assembly of surface ligands. Gold atoms under these conditions behave very differently when compared with atoms in an ideal slab structure.[10−12] The nanorod's surface structure is closely related to its surface activity;[2] hence, resolving geometric features is crucial. Simulations on flat surfaces are useful for studying some types of molecular interactions,[13,14] but they cannot capture phenomena governed by local features such as defects and geometric curvatures. A multifaceted model can examine how the boundary between two surfaces, or a corner between two facets, affects the binding of ligands. These important aspects have been neglected in previous simulations but are crucial to understanding the dynamic growth of self-assembled monolayers (SAMs) on nanorods. To add to this already complicated system, the chemisorptions process of alkanethiol ligands can induce strong changes to the gold substrates and surface reorganization, leading to potential surface defect structures.[15] Alkanethiolates will behave differently when placed next to a surface defect due to different sulfur−gold interactions.[16] Such defects are a critical factor in determining the final assembly of the SAMs on nanoparticles.[17] The significance of multifaceted structure not only applies to GNRs but also to other important octahedron nanoparticles, and hence, it is a generic aspect of nanochemistry.

The organization of this paper is as follows. Section 2 describes the computational methods and the simulation programs. Section 3 discusses the key results and the important conclusions that can be drawn from them. Finally section 4 summarizes the

Received: March 22, 2013
Revised: September 11, 2013

   dx.doi.org/10.1021/jp4028589 | *J. Phys. Chem. B* XXXX, XXX, XXX−XXX

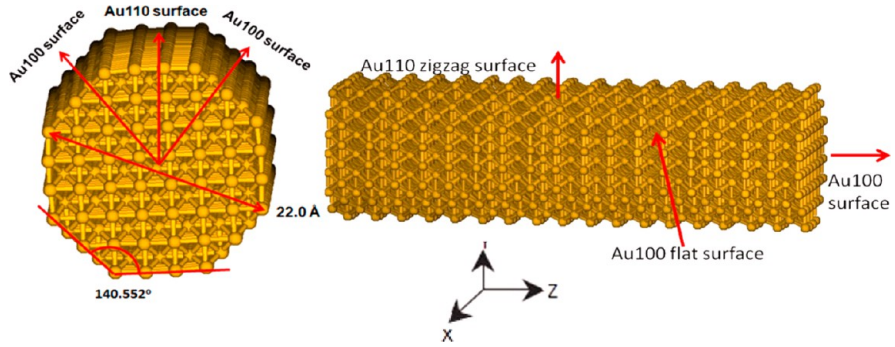

Figure 1. Structure of one-dimensional gold nanorod. The left figure shows the front view of the nanorod; note the alternate Au100 and Au110 facets. The right figure shows the side view of the gold nanorod; note the zigzag surface on Au110 and the coordinate system. *Z* represents the axial direction of the nanorod.

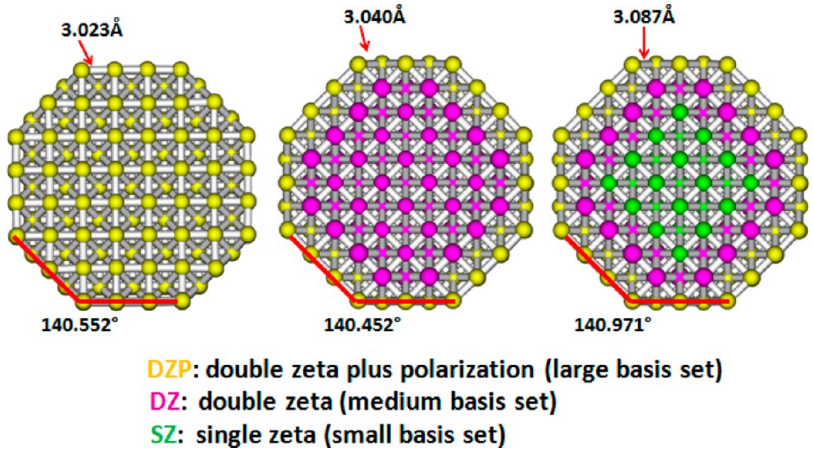

Figure 2. Color coded simulation structure of the multiple basis sets of the gold nanorod. The inner angle and average bond length showing the similarity of simulation results are also indicated at the bottom and top of the figure, respectively.

significance of the simulation results and implications for future work. In general, the study of GNRs' chemical and mechanical properties is important to the development of nanoelectromechanical devices (NEM). This information will also serve as a basis for future studies of Au100 and Au520 surfaces.[18]

2. MATERIALS AND METHOD

The simulations of the 1-dimensional GNR model systems were based on first-principles density functional theory (DFT), implemented using SIESTA's code.[19] For this simulation, the Perdew−Burke−Ernzerhof (PBE) generalized gradient approximation (GGA) exchange correlation functionals and the Improved Troullier−Martins norm-conserving pseudopotentials were adopted for all atoms in the system.[20,21] The reference configuration for gold is [Xe] $5d^{10}$ $6s^1$, that for sulfur is [Ne] $3s^2$ $3p^4$, that for carbon is [He] $2s^2$ $2p^2$, and that for hydrogen is $1s^1$.[22] The cutoff radii are 2.35 Å for gold, 1.70 Å for sulfur, 1.25 Å for carbon, and 1.25 Å for hydrogen.[22] The 1-dimensional GNR follows an octagonal structure with alternate Au100 and Au110 facets.[23] The nanorod has a cross section length around 22.0 Å, and it is assumed to be infinite along the Au100 surface or *Z* direction, as indicated in Figure 1. The crystal structure parameters are as follows: A = 50.4698 Å, B = 50.4698 Å, C = 8.1566 Å, and $\alpha = \beta = \gamma = 90.00°$. The symmetry group for the gold nanorod before optimization is $P4/MMM$ ($D4H-1$), this is used to obtain the band line information for the vibration spectrum simulation.

There are three different basis set configurations for the GNR model. For the first configuration, all gold atoms were simulated with numerical double-ζ plus polarization (DZP). The second configuration had a DZP basis for the outermost layers and used double-ζ (DZ) for all inner atoms. For the last configuration, all gold atoms used single-ζ (SZ), except the outermost layer and the second outermost layer, which used DZP and DZ, respectively. The color-coded atomic structure of the GNR with different basis sets can be seen in Figure 2.

The size of the crystal cell was fixed for each individual cross section with the atomic positions optimized with respect to the total energy minimization without any constraint on the symmetry for each of the cross sections. The infinitely long gold nanorod would exhibit translational symmetry. The molecular structure is considered optimized, when the force experienced by each atom is less than 0.008 eV/Å. A 20.0 Å cutoff was employed for the *k*-point sampling in structure optimization calculations. To establish stability, the phonon dispersion relations were calculated based on the scheme proposed by Kunc and Martin.[24] First, 1 × 1 × 3 supercells were created to limit the forces inside the cells with all irreducible directions within the cells that were searched. Second, each atom was displaced perpendicular to the *X*, *Y*, and *Z* planes to calculate the forces exerted on all atoms by the displacement. The results were used to construct the force constant matrix and then used to calculate the dynamical matrix for the primitive cell for different **k** vectors along the high symmetry axes. The frequencies of the phonon modes for each *k* were calculated from the square roots of the eigenvalues for the dynamical matrix. This imaginary

dx.doi.org/10.1021/jp4028589 | J. Phys. Chem. B XXXX, XXX, XXX−XXX

frequency indicates instability of the phases, because it corresponded to directions of barrier-less phase transitions.

Once the stability of GNR was determined, other important physical and chemical properties were studied. Finite temperature, NVT *ab initio* molecular dynamics (AIMD) simulation was used to study the system's thermal stability at 300 K, with number of moles, volume, and temperature conserved.[25] This temperature was chosen to resemble the ambient condition. The Nosé–Hoover thermostat was used as a temperature control.[26] The AIMD simulation took 420 steps with 1.0 fs for each step. Also, the nanorod band energies were calculated along high symmetry directions such as Γ, X, L, and W.

The stress and strain relationship of this nanorod structure was also considered. The matrix equation below shows the linear elastic stress tensor of an orthotropic material,[27] relevant to the mechanics of nanorods

$$\begin{bmatrix} \varepsilon_{xx} \\ \varepsilon_{yy} \\ \varepsilon_{zz} \\ 2\varepsilon_{yz} \\ 2\varepsilon_{zx} \\ 2\varepsilon_{xy} \end{bmatrix} = \begin{bmatrix} \frac{1}{E_x} & \frac{-v_{yx}}{E_y} & \frac{-v_{zx}}{E_z} & 0 & 0 & 0 \\ \frac{-v_{xy}}{E_x} & \frac{1}{E_y} & \frac{-v_{zy}}{E_z} & 0 & 0 & 0 \\ \frac{-v_{xz}}{E_x} & \frac{-v_{yz}}{E_y} & \frac{1}{E_z} & 0 & 0 & 0 \\ 0 & 0 & 0 & \frac{1}{G_{yz}} & 0 & 0 \\ 0 & 0 & 0 & 0 & \frac{1}{G_{zx}} & 0 \\ 0 & 0 & 0 & 0 & 0 & \frac{1}{G_{xy}} \end{bmatrix} \times \begin{bmatrix} \sigma_{xx} \\ \sigma_{yy} \\ \sigma_{zz} \\ \sigma_{yz} \\ \sigma_{zx} \\ \sigma_{xy} \end{bmatrix}$$

where σ_{xx}, σ_{yy}, and σ_{zz} are the normal stresses in the X, Y, and Z directions, σ_{yz}, σ_{zx}, and σ_{xy} represent the shear stresses, ε_{ij} is the strain, E_i is the Young's modulus along the i^{th} axis, G_{ij} is the shear modulus in plane j with surface normal in the i direction, and v_{ij} is Poisson's ratio of extension in the i direction over the contraction in the j direction. For our simulations, we intentionally introduced a small strain (linear elasticity regime) in the aixal or Z direction; see Figure 1. After the structure was optimized based on the induced strain, the stress tensor field was calculated. Using the crystal cell size of the newly optimized structure and the stress tensor field, we were able to find the Poisson's ratio and the Young's modulus.

Once the chemical and physical properties of the gold nanorod were characterized, it was also important to study how it would interact with SAMs on its surface. Alkanethiol ligands ranging from methanethiol to pentanethiol were added to the surface. The ligands were arranged with a higher packing density on the high energy Au110 surface, with three ligands binding to each facet. Two ligands were added to the more stable Au100 surface. The structure of the final SAM assembly on a multifaceted structure and ligand cant angles on different surfaces were obtained.

3. RESULTS AND DISCUSSIONS

Three different basis set configurations were tested to design a method that can improve the simulation speed without compromise in accuracy. In our earlier work,[28] we studied the electron density distribution of the gold–thiol interface. It was noted that only the top layer of gold atoms contributed to the charge transfer to the sulfur atom.[28] This result strongly suggests that a smaller basis can be used to simulate inner gold atoms, as they do not contribute to the structure of the SAM. The requirement is that the final optimized structure of the octagonal nanorod should not be altered by the change of basis. For the actual simulation, the run time for each cycle for the first basis configuration is 352 s, that for the second configuration is 211 s, and that for the third configuration is only 106 s. By adopting this multibasis approach, we have improved the computational efficiency by more than a factor of 3 while maintaining the structural integrity of the nanorod. As we can see from Figure 2, the angles of the octagonal nanorod and the average bond length between the gold atoms on the outer layer are very similar. The average bond length for the DZP/DZ/SZ basis is 3.087 Å, and the average is 141° for the internal angle. For DZP, the averages are 3.023 Å and 140°. The deviation between the two results is less than 2%.

Phonon dispersion calculations were used to study the stability of the nanorod system. Based on Figure 3A, we can see that the GNR is dynamically stable without negative frequency nodes. In comparison with Figure 3C, the acoustical nodes for the nanorods are more complex than for a fcc gold crystal, as they do not have any overlap. Figure 4 plots the band gap for the nanorod system. This shows us that the nanorod is a good conducting material. From the thermal stability study, it was found the nanorod is stable at temperatures around 300 K, as can be seen in Figure 5. It is also important to note that the nanorod will undergo significant surface reorganization during the process. This agrees well with experimental findings that the gold nanorod will change its aspect ratio as a function of temperature during synthesis.[11,16] An initial and final structure comparison is presented in Figure 6.

After characterizing the GNRs' chemical properties, its mechanical properties were also studied, especially how the GNR will respond to normal force in the axial or Z direction. When compressed in the Z direction, the nanorod will expand in the X and Y directions. The changes in stress tensor and unit cell size in the X and Y directions are identical, indicating that the octagonal nanorod is an orthotropic material; the results are tabulated in Table 3. Based on the coordinates of Figure 1, the X–Y surface is the plane of symmetry. A small strain load was introduced to keep the effect in the linear elastic regime. It is important to point out that even when the strain was very small, the nanorod already started generating internal shear stress in the Y–Z surface. Many stress and strain tests on gold nanorod surfaces have indicated that the largest shear stress occurs off-axis of the applied strain.[29] This agrees very well with our simulation results. The onset of shear stress on the Y–Z surface indicates that a defect structure would most likely be formed first along the radial directions rather than the axial direction. A similar effect was found in the next section with ligand-induced stress. The calculated Poisson ratio is close to 0.76 (Table 2). The mechanical properties of the gold nanorod are heavily dependent on its nanostructure and size. The Young's modulus for the axial direction along the Au100 surface is 207 kbar, and that for the axial direction is 631 kbar (Table 1). The experimental value of Young's modulus in the Au100 surface growth direction is 310 ± 10 kbar, and it is 640 ± 20 kbar for the growth in the Au110 surface direction.[23] For the radial direction with a mixed Au100 and Au110 surface, the value for Young's modulus agrees very well with the experimental values. For the Au100 surfaces in the Z direction, the calculated Young's modulus is smaller than the experimental value. The discrepancy is due to the fact that the simulation model is much thinner than the experimental GNR.

The GNR response to alkanethiol ligand binding is very different from the simple slab surface structure. Many experiments have shown that the surface of a gold nanorod will undergo significant surface reconstruction to achieve a lower energy state.[3,10,12,30] The ligands will arrange themselves to occupy

dx.doi.org/10.1021/jp4028589 | J. Phys. Chem. B XXXX, XXX, XXX–XXX

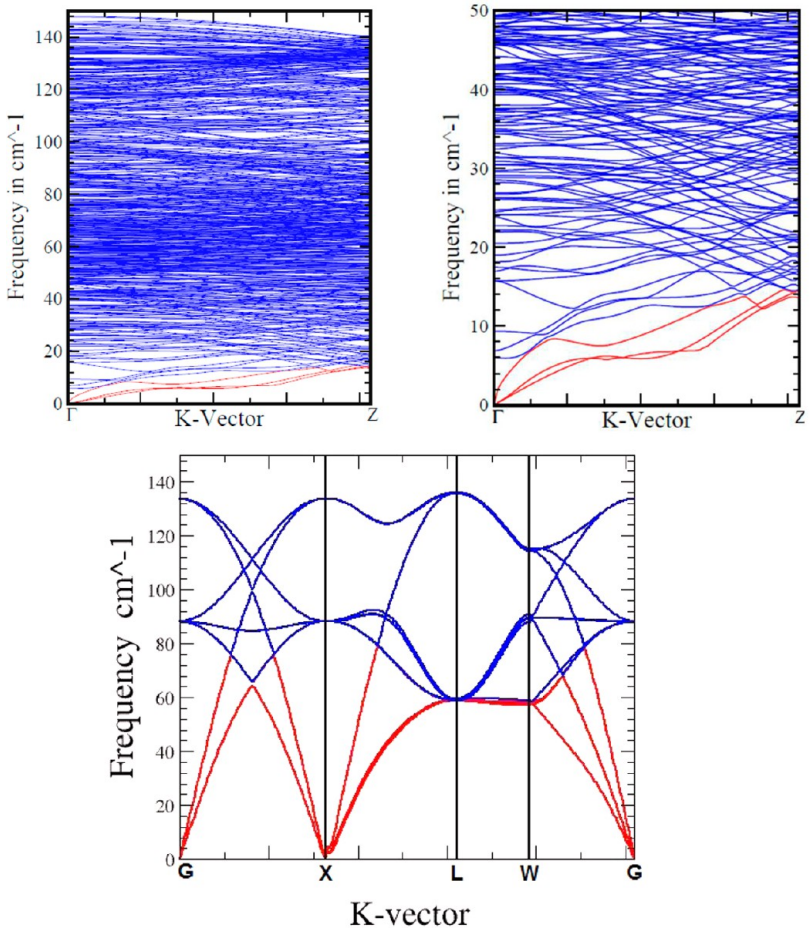

Figure 3. Au nanorod is dynamically stable without negative frequency modes. Red indicates the acoustic node, and blue is the optical node. (A, left) All the phonon nodes. (B, right) All the phonon nodes with frequencies less than 50 cm^{-1}. (C) Phonon dispersion of a single fcc gold crystal. The acoustic node in red shows strong overlap in comparison with the nodes for a nanorod.

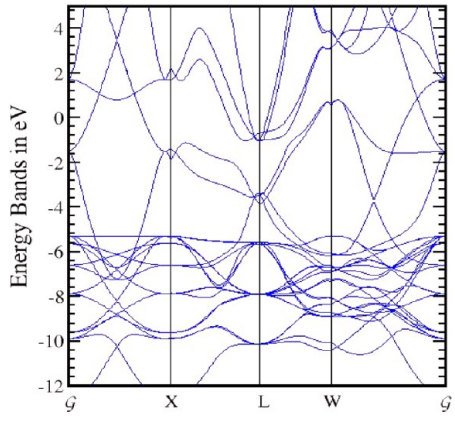

Figure 4. Energy band plot of the GNR. The band structures show no band gaps, indicating the nanorod is a good conducting material.

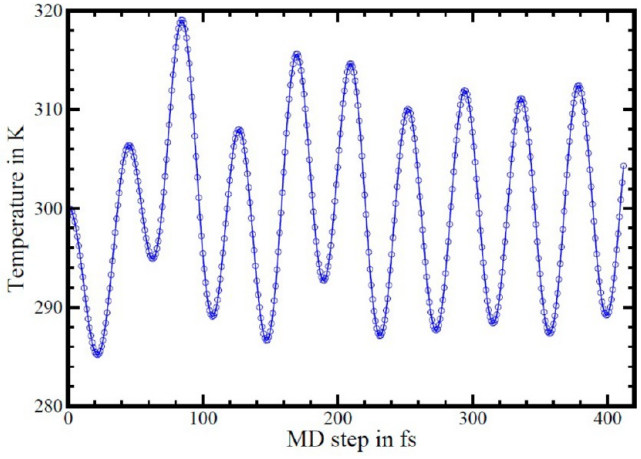

Figure 5. Molecular dynamic simulation of a gold nanorod at 300k. Each point indicates the system temperature at a specific time; the average system temperature would be 300 K.

empty spaces around the GNR. This will lead to a significant degree of bending, especially in the ligands located at the corner positions. The average cant angle is 29° for ligands on the Au110 gold facets, away from the edge. The optimized molecular model can be found in Figures 7 and 8. For the Au100 surface, the ligand cant angle decreased as ligand length increased. This is because the two ligands located around the edge of Au100 surfaces have to bend toward each other. Since the free space between them is limited, longer ligands will have a smaller cant angle due to ligand−ligand interactions. Therefore, the shorter ligands were able to achieve a cant angle of approximately 30°. Figure 9 shows the correlation between ligand cant angle and ligand length. The ligand structure at the boundary between two surfaces is very different. The gold substrate to ligand interactions created a point defect at the surface of Au110, as indicated in point A in

dx.doi.org/10.1021/jp4028589 | J. Phys. Chem. B XXXX, XXX, XXX−XXX

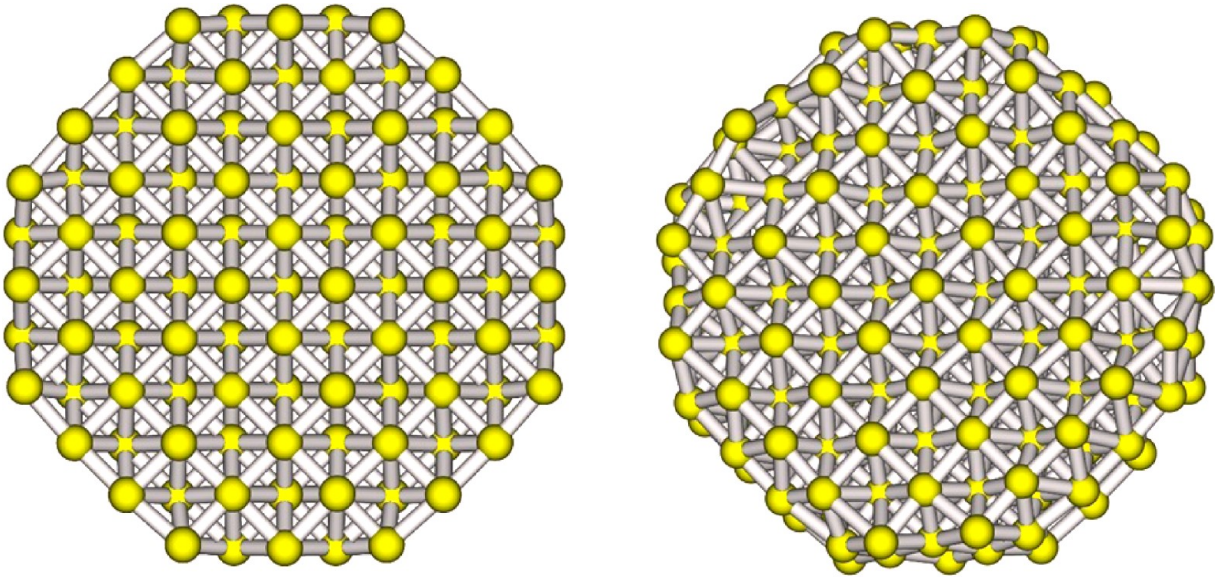

Figure 6. Initial structure of a gold nanorod and final structure of a gold nanorod at 420 fs. The nanorod will undergo significant surface reorganization after thermal heating.

Table 1. Young's Modulus of Gold Nanorod

	E_x (kbar)	E_y (kbar)	E_z (kbar)
Young's modulus	207	207	631

Table 2. Poisson's Ratio of Gold Nanorod

	ν (equatorial direction)	ν (axial direction)
Poisson's ratio	1.0	0.76

Table 3. Stress Tensor Field in Voigt's Notation

induced strain	normal stress (σ_{xx}, σ_{yy}, σ_{zz})	shear stress (σ_{xx}, σ_{yy}, σ_{zz})
0.25%	0.11, 0.11, −0.33	0.01, 0.00, 0.00
0.12%	0.09, 0.09, −0.44	0.01, 0.00, 0.00

Figure 7 by the broken gold to gold bond. This point defect allowed the ligand at the boundary to achieve a cant angle of 40°. For the more stable Au100 surface, the bond breaking occurs at the second layer of the gold nanorod, as indicated in point B in Figure 7. This inner defect will make the surface atoms move closely toward each other, creating a small island with high surface density. There are two reasons why the different facets responded differently to ligand binding. The Au110 surface is less stable when compared with the Au100 surface.[12] It takes less energy for the gold atom at the Au110 surface to break a bond with neighboring atoms. In this way, it can create a positive concavity that expands the surface length and gives the ligands more spaces. The energy cost for creating this defect can be compensated by higher adsorption energy. Earlier simulation and theoretical studies have shown that the ligand adsorption energy is higher for ligands with cant angle greater than 30° but less than 40°.[13] Since the Au100 surface is more stable, the energy required for a surface atom to break its bond would be higher. The bond breaking at the second layer actually helps the surface atom to create a negative concavity to assist the ligands bending inward to occupy the middle free space. These results agree well with earlier experimental findings. It is known that the Au100 surfaces on a gold nanorod can have atom height surface defects while still maintaining stability.[12,31] The simulation

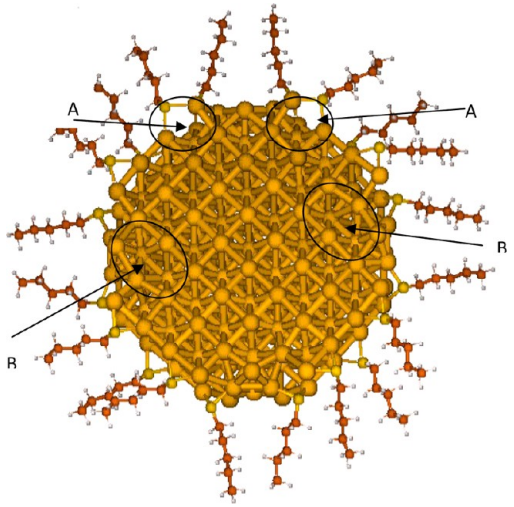

Figure 7. Optimized molecular model for gold nanorods with pentanethiol as surface ligands. Point A indicates surface defects on the gold nanorod Au110 surfaces. Point B shows the internal defects occurring at the second layer of the Au100 surfaces.

results provide a possible explanation for this behavior. The Au100 surface can have bond breaking in the inner layer and create a surface island, if this helps stabilize the whole system, as in the case of alkanethiolate binding.[31] For the Au110 surface, surface bond breaking and forming is more likely, if the reorganization process can achieve a lower energy state. This can be seen in the case of missing row reconstruction, where the Au110 surface will displace a whole row of atoms at the surface.[12]

The distance between the two gold atoms with a broken bond increased to 3.56 Å. This created two different types of Au110 side lengths. The average length for longer ones containing a point defect is 9.76 Å. The original side length for a Au110 surface without a surface defect is around 9.26 Å. By approximating the side length as a parabola, the horizontal extension of the rod can be estimated. For the longer sides, the extended area is around 9.12 Å^2. Since there are four Au110 sides, the total increase is 36.48 Å^2, an increase of 9% from the original total

dx.doi.org/10.1021/jp4028589 | J. Phys. Chem. B XXXX, XXX, XXX−XXX

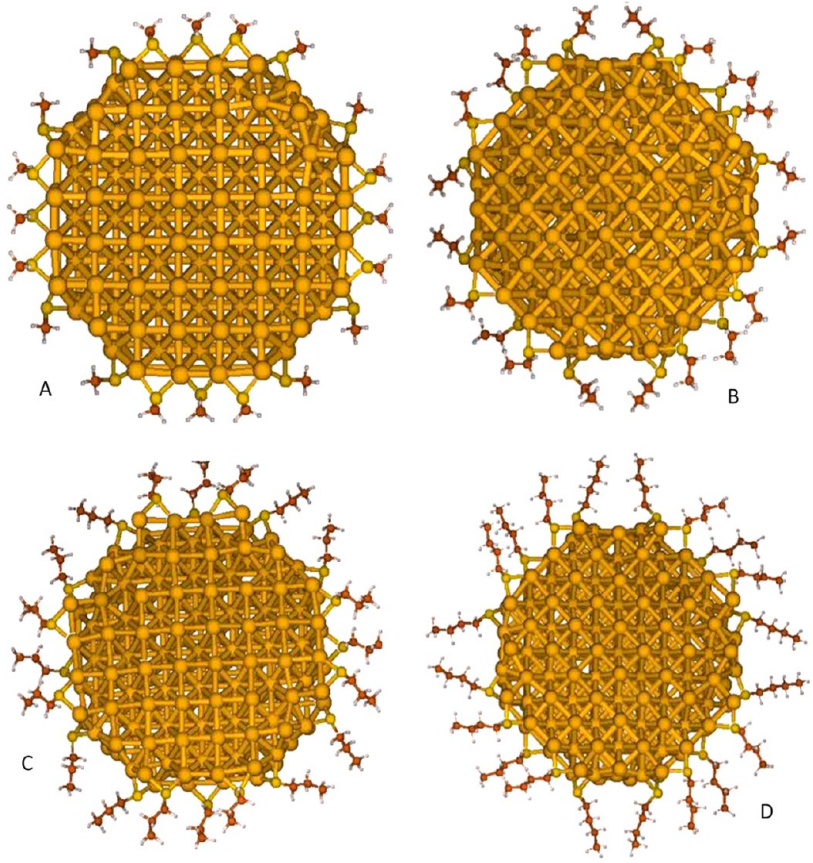

Figure 8. Molecular models of gold nanorods with different ligands: A, methanethiol; B, ethanethiol; C, propanethiol; D, butanethiol.

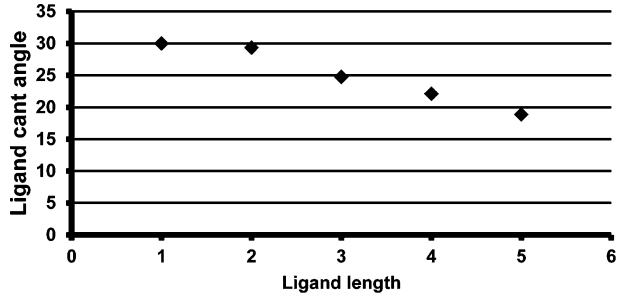

Figure 9. Plot of ligand cant angle versus ligand length on Au 100.

cross-sectional area of approximately 402.45 Å^2. Previously, simulations have shown that heating the Au100 and Au110 surfaces can change the surface atom structure and, in turn, can affect the inner layer of gold atoms. Our simulation results have proved that ligand binding can have a similar effect on the surfaces of GNRs.[16]

4. CONCLUSIONS

The paper presents for the first time a novel simulation approach to study multifaceted gold nanorods. The gold nanorod can be accurately represented by a multibasis approach. With its high degree of accuracy, the hybrid basis system can serve as an efficient platform for future nanorod studies. Phonon dispersion simulations were used to prove the dynamic stability of gold nanorods. AIMD, NVT simulations have demonstrated the thermostability of the model. Unlike the slab structures where the surface structure does not change much, the nanorods have more fluid surfaces that will rearrange themselves to respond to external conditions. When the nanorod is under compression in the axial direction, it responded as an orthotropic material by expanding uniformly along the radial direction. When the rod is bonded with alkanthiol ligands, the surface gold atoms will rearrange themselves to expand the total surface available to the ligands. This is achieved by creating surface defects on the Au110 surface and inner layer defects on the Au100 surfaces. The resulting positive and negative concavities help the ligands arrange themselves further apart and reduce internal strain. The simulation results have allowed substantial progress to be made toward understanding the physical and chemical properties of gold nanorods as well as their interactions with surface ligands.

AUTHOR INFORMATION

Corresponding Author

*Ph: +1-514-398-4196 Fax: +1-514-398-6678. E-mail: alejandro.rey@mcgill.ca.

Notes

The authors declare no competing financial interest.

ACKNOWLEDGMENTS

This work is supported by grants from the Natural Science and Engineering Research Council (NSERC), McGill Institute for Sustainability in Engineering and Design (ISEAD), and Le Fonds de recherche du Québec—Nature et technologies (FQNRT).

REFERENCES

(1) Murphy, C. J.; Gole, A. M.; Stone, J. W.; Sisco, P. N.; Alkilany, A. M.; Goldsmith, E. C.; Baxter, S. C. Gold Nanoparticles in Biology: Beyond Toxicity to Cellular Imaging. *Acc. Chem. Res.* **2008**, *41*, 1721–1730.

(2) Huang, X.; Neretina, S.; El-Sayed, M. A. Gold Nanorods: From Synthesis and Properties to Biological and Biomedical Applications. *Adv. Mater.* **2009**, *21*, 4880−4910.
(3) Carbó-Argibay, E.; Rodríguez-González, B.; Pacifico, J.; Pastoriza-Santos, I.; Pérez-Juste, J.; Liz-Marzán, L. M. Chemical Sharpening of Gold Nanorods: The Rod-to-Octahedron Transition. *Angew. Chem.* **2007**, *119*, 9141−9145.
(4) Lu, Y.; Song, J.; Huang, J. Y.; Lou, J. Fracture of Sub-20nm Ultrathin Gold Nanowires. *Adv. Funct. Mater.* **2011**, *21*, 3982−3989.
(5) Wang, Z. L.; Mohamed, M. B.; Link, S.; El-Sayed, M. A. Crystallographic Facets and Shapes of Gold Nanorods of Different Aspect Ratios. *Surf. Sci.* **1999**, *440*, 809−814.
(6) Yu, Y.; Chang, S.-S.; Lee, C.-L.; Wang, C. R. C. Gold Nanorods: Electrochemical Synthesis and Optical Properties. *J. Phys. Chem. B* **1997**, *101*, 6661−6664.
(7) Barnard, A. S. Shape, Orientation, and Stability of Twinned Gold Nanorods. *J. Phys. Chem. C* **2008**, *112*, 1385−1390.
(8) Milette, J.; Toader, V.; Reven, L.; Lennox, R. B. Tuning the Miscibility of Gold Nanoparticles Dispersed in Liquid Crystals Via the Thiol-for-DMAP Reaction. *J. Mater. Chem.* **2011**, *21*, 9043−9050.
(9) Pérez-Juste, J.; Pastoriza-Santos, I.; Liz-Marzán, L. M.; Mulvaney, P. Gold nanorods: Synthesis, Characterization and Applications. *Coord. Chem. Rev.* **2005**, *249*, 1870−1901.
(10) Goris, B.; Bals, S.; Van den Broek, W.; Carbó-Argibay, E.; Gómez-Graña, S.; Liz-Marzán, L. M.; Van Tendeloo, G. Atomic-scale Determination of Surface Facets in Gold Nanorods. *Nat. Mater.* **2012**, *11*, 930−935.
(11) Mohamed, M. B.; Ismail, K. Z.; Link, S.; El-Sayed, M. A. Thermal Reshaping of Gold Nanorods in Micelles. *J. Phys. Chem. B* **1998**, *102*, 9370−9374.
(12) Wang, Z. L.; Gao, R. P.; Nikoobakht, B.; El-Sayed, M. A. Surface Reconstruction of the Unstable {110} Surface in Gold Nanorods. *J. Phys. Chem. B* **2000**, *104*, 5417−5420.
(13) Yourdshahyan, Y.; Rappe, A. M. Structure and Energetics of Alkanethiol Adsorption on the Au(111) Surface. *J. Chem. Phys.* **2002**, *117*, 825−833.
(14) Tachibana, M.; Yoshizawa, K.; Ogawa, A.; Fujimoto, H.; Hoffmann, R. Sulfur−Gold Orbital Interactions which Determine the Structure of Alkanethiolate/Au(111) Self-Assembled Monolayer Systems. *J. Phys. Chem. B* **2002**, *106*, 12727−12736.
(15) Ramírez, E. A.; Cortés, E.; Rubert, A. A.; Carro, P.; Benítez, G.; Vela, M. E.; Salvarezza, R. C. Complex Surface Chemistry of 4-Mercaptopyridine Self-Assembled Monolayers on Au(111). *Langmuir* **2012**, *28*, 6839−6847.
(16) Wang, Y.; Teitel, S.; Dellago, C. Surface-driven Bulk Reorganization of Gold Nanorods. *Nano Lett.* **2005**, *5*, 2174−2178.
(17) Giomi, L.; Bowick, J. M.; Ma, X.; Majumda, A. Molecular Tilt on Monolayer-protected Nanoparticles. *Europhys. Lett.* **2012**, *97*, 36005−36010.
(18) Goris, B.; Bals, S.; Van den Broek, W.; Carbó-Argibay, E.; Gómez-Graña, S.; Liz-Marzán, L. M.; Van Tendeloo, G. Atomic-scale Determination of Surface Facets in Gold Nanorods. *Nat. Mater.* **2012**, *11*, 930−935.
(19) Jose, E. A.; Gale, J. D.; Garcia, A.; Junquera, J.; Ordejon, P.; Sanchez-Portal, D. The SIESTA Method of Ab Initio Order-N Materials Simulation. *J. Phys.: Condens. Matter* **2002**, *14*, 2745−2779.
(20) Perdew, J. P.; Burke, K.; Ernzerhof, M. Generalized Gradient Approximation Made Simple. *Phys. Rev. Lett.* **1996**, *77*, 3865−3868.
(21) Liu, R.; Ke, S.-H.; Baranger, H. U.; Yang, W. Negative Differential Resistance and Hysteresis Through an Organometallic Molecule From Molecular-Level Crossing. *J. Am. Chem. Soc.* **2006**, *128*, 6274−6275.
(22) Castro, A.; Appel, H.; Oliveira, M.; Rozzi, C. A.; Andrade, X.; Lorenzen, F.; Marques, M. A. L.; Gross, E. K. U.; Rubio, A. Octopus: A Tool For The Application of Time-Dependent Density Functional Theory. *Phys. Status Solidi B* **2006**, *243*, 2465−2488.
(23) Petrova, H.; Perez-Juste, J.; Zhang, Z.; Kosel, T.; Hartland, G. V. Crystal structure dependence of the elastic constants of gold nanorods. *J. Mater. Chem.* **2006**, *16*, 3957−3963.
(24) Kunc, K.; Martin, R. M. Ab Initio Force Constants of Gas: A New Approach to Calculation of Phonons and Dielectric Properties. *Phys. Rev. Lett.* **1982**, *48*, 406−409.
(25) Elliott, J. A.; Hanna, S.; Elliott, A. M. S.; Cooley, G. E. Atomistic simulation and molecular dynamics of model systems for perfluorinated ionomer membranes. *Phys. Chem. Chem. Phys.* **1999**, *1*, 4855−4863.
(26) Nose, S. A Unified Formulation of The Constant Temperature Molecular Dynamics Methods. *J. Chem. Phys.* **1984**, *81*, 511−519.
(27) Lempriere, B. Poisson's Ratio In Orthotropic Materials. *AIAA J.* **1968**, *6*, 2226−2227.
(28) Hu, H.; Reven, L.; Rey, A. D. Ab initio DFT Study of 6-mercapto-hexane SAMs: Effect Of Au Surface Defects On The Monolayer Assembly. *Mol. Simul.* **2012**, *39*, 1−7.
(29) Kelchner, C. L.; Plimpton, S. J.; Hamilton, J. C. Dislocation nucleation and defect structure during surface indentation. *Phys. Rev. B* **1998**, *58*, 11085−11088.
(30) Carbó-Argibay, E.; Rodríguez-González, B.; Gómez-Graña, S.; Guerrero-Martínez, A.; Pastoriza-Santos, I.; Pérez-Juste, J.; Liz-Marzán, L. M. The Crystalline Structure of Gold Nanorods Revisited: Evidence for Higher-Index Lateral Facets. *Angew. Chem., Int. Ed.* **2010**, *49*, 9397−9400.
(31) Love, J. C.; Estroff, L. A.; Kriebel, J. K.; Nuzzo, R. G.; Whitesides, G. M. Self-Assembled Monolayers of Thiolates on Metals as a Form of Nanotechnology. *Chem. Rev.* **2005**, *105*, 1103−1170.